RESEARCH ARTICLE | JANUARY 06 2025

Telecom source of tunable polarization-entanglement distribution up to 100-km for multi-user QKD over metro-area fiber-optic networks

Vikash Kumar Yadav ; Vivek Venkataraman; Joyee Ghosh

APL Quantum 2, 016102 (2025)
https://doi.org/10.1063/5.0241324

Telecom source of tunable polarization-entanglement distribution up to 100-km for multi-user QKD over metro-area fiber-optic networks

Cite as: APL Quantum 2, 016102 (2025); doi: 10.1063/5.0241324
Submitted: 30 September 2024 • Accepted: 6 December 2024 •
Published Online: 6 January 2025

Vikash Kumar Yadav,[1,a] Vivek Venkataraman,[1,2,b] and Joyee Ghosh[1,c]

AFFILIATIONS

[1] Quantum Photonics Lab, Department of Physics, Indian Institute of Technology Delhi, New Delhi 110016, India
[2] Department of Electrical Engineering, Indian Institute of Technology Delhi, New Delhi 110016, India

[a] Electronic mail: vikky11295@gmail.com
[b] Electronic mail: vivekv@ee.iitd.ac.in
[c] Author to whom correspondence should be addressed: joyee@physics.iitd.ac.in

ABSTRACT

The scalability of quantum communication networks requires compact, fiber-integrated, easy-to-deploy, and efficient wavelength-division-multiplexed (WDM) sources for multi-user secure key distribution. Here, we demonstrate such a multi-channel source of polarization-entangled photon pairs in the low-loss telecom C-band based on type-0 spontaneous parametric downconversion in a fiber-coupled Zn-indiffused MgO-doped periodically poled lithium-niobate (MgO:PPLN) ridge waveguide in the Sagnac configuration. The source can be easily tuned to generate the $|\Phi^+\rangle$ or $|\Phi^-\rangle$ Bell state in 14 channel pairs of the International Telecommunication Union dense WDM (100-GHz spacing) grid around 1550-nm with a raw fidelity of $\gtrsim$89%, with a maximum value of $\gtrsim$94%. The raw concurrence is $\gtrsim$0.8 for both Bell states in all channel pairs, and the observed S-parameter (>2.56 ± 0.04 in all 14-channel pairs) shows a strong violation of CHSH-Bell's inequality. The source's suitability for long-distance entanglement transmission is also demonstrated by the successful transfer of entangled photons up to 100 km while maintaining fidelity >85% and quantum bit error rate <9%. The effect of polarization mode dispersion on entanglement distribution among remote users is also studied in detail. All these performance metrics are measured using conventional room-temperature semiconductor-based single-photon avalanche detectors, and these are the best reported with these detectors. Our highly flexible source can support up to ~40 user pairs to communicate simultaneously, and it can be easily deployed into the current metro-area fiber-optic telecom infrastructure to form a complete WDM-based quantum communication network.

I. INTRODUCTION

Quantum communication networks enable widespread connectivity for multi-user communication and secret key distribution.[1,2] A multi-channel entangled photon pair source could be the key to the development of such a realistic quantum network.[1–4] The entangled photons have wide applications in various quantum technologies such as trusted-node free secure communication,[5,6] quantum key distribution (QKD),[7–9] entanglement swapping,[10,11] and quantum sensing.[12–14] Technologies such as QKD and entanglement distribution are now well-established, and successful transmission of polarization-entangled photons over hundreds of kilometers via optical fiber cables[15,16] and secure key generation between remote users[7,16,17] has been demonstrated. Despite the advancement in quantum light sources based on spontaneous parametric downconversion (SPDC)[18–20] and spontaneous four-wave-mixing (SFWM),[21,22] the development of large-scale, fully connected quantum networks has remained elusive because of the applicability of such sources mostly being limited to a single pair of communicating parties/users. In this regard, a multi-channel WDM source of polarization-entangled photon pairs could be one of the potential candidates for the establishment of a large

metropolitan-scale quantum communication network. Different sources of multi-user communication have been proposed in the last two decades; the source proposed by Ref. 3 potentially supports 44 channel pairs, but entanglement was characterized in only six channel pairs; Ref. 4 has shown polarization entanglement in four channel pairs, Ref. 23 has shown hyper-entanglement in five channel pairs, and Refs. 1 and 2 have shown the entanglement in 6 and 8 channel pairs, respectively. The above sources utilize a periodically poled lithium niobate (PPLN) crystal/waveguide and generate a $|\Phi^+\rangle$ Bell state; Ref. 3 used a 1-mm long PPLN in the Sagnac loop in a free space setup, Ref. 4 used two 30-mm long PPLN crystals arranged in a Mach–Zehnder interferometer in a free space setup, Ref. 23 used a 38-mm long PPLN in the Sagnac loop in a fiber-integrated setup, and Refs. 1 and 2 used a 40-mm and 50-mm long PPLN crystal in the Sagnac loop in free space, respectively, for polarization-entangled photon pair generation at telecom wavelengths. Recently, more than 15 parallel polarization entangled wavelength channel pairs in the telecom band were demonstrated to create a wide-area quantum network.[24–26] The above-mentioned sources are either limited to a few users and/or are not compact/fiber-integrated and difficult to deploy outside the laboratory and/or have not completely characterized all performance metrics of the source important for applicability in long-distance (metropolitan-scale) networks. The scalability of a WDM-based quantum communication network requires an easily deployable, compact, efficient, and stable broadband/multi-channel source of polarization-entangled photons with high brightness, tight spectral correlation, and negligible crosstalk between corresponding channel pairs.

Here, we demonstrate and comprehensively characterize such a fully fiber-integrated multi-user source of polarization-entangled photons in the lowest fiber-loss telecom C-band based on a 40-mm long Zn-indiffused MgO:PPLN ridge waveguide. Spectrally correlated photon pairs with high spectral brightness and large bandwidth are produced by the type-0 phase-matched lithium-niobate through high nonlinearity and wide phase-matching.[27] We employ the waveguide in Sagnac configuration to generate broadband polarization-entangled photon pairs around the telecom wavelength of 1550 nm (spanning the C- and L-bands)[28] and demultiplex them using a standard arrayed waveguide grating (AWG) into the dense WDM (DWDM) International Telecommunication Union (ITU) grid with 100-GHz channel spacing. According to the user's demand, the source can generate either $|\Phi^+\rangle$ or $|\Phi^-\rangle$ Bell state, and the output state can be easily tuned with the help of a fiber polarization controller.

We characterize various entanglement witness parameters, such as two-photon interference, violation of CHSH-Bell's inequality, and quantum state fidelity, in 14 ITU wavelength channel pairs and show that all of them simultaneously provide high-fidelity entangled states. Our source generates 14 independent bipartite polarization-entangled states, which enables 14 different user pairs to access the source simultaneously for trusted-node free multi-user quantum communication and key distribution.[1,4,5,16] Although we demonstrate entanglement across 14-channel pairs, it can be further extended to ~40-user pairs since the broadband photon pair emission spectrum is still not fully utilized after demultiplexing through our C-band 32-channel (100-GHz spacing) AWG. The source does not require any active stabilization and can be easily deployed in a WDM-based quantum communication network utilizing standard fiber-optic telecom infrastructure. We assess the source for long-distance (metropolitan-scale) entanglement transmission using fiber spools and study the effect of polarization mode dispersion (PMD) on entanglement distribution. A successful transfer of entangled photons up to 100 km distance apprises the compatibility of our source for long-distance multi-user QKD and communication in a fiber-optic quantum network.

Here, we show the full entanglement characterization in 14 parallel wavelength channel pairs of a fully fiber-integrated polarization-entangled photon-pair source and report the best performance metrics to date with standard single-photon avalanche detectors (APDs). The proposed source can be easily deployed in the current metro-area fiber-optic infrastructure to scale up the quantum communication network for multi-user QKD and communication. Potentially, the source can also be used for information processing, quantum metrology, and entanglement swapping.

II. EXPERIMENTAL SETUP

Figure 1 shows the experimental setup for generating and characterizing polarization-entangled photon pairs for multi-user quantum communication and secret key distribution. A continuous wave (CW) tunable pump laser at 775 nm (Toptica Photonics AG), whose power can be controlled through an inline variable optical attenuator (VOA), is used to pump a fiber-pigtailed 40-mm long Zn-indiffused MgO:PPLN ridge waveguide (Covesion Ltd.) placed in the Sagnac configuration. The waveguide is type-0 phase-matched for degenerate downconversion, i.e., 775 nm (pump, V-pol) → 1550 nm (signal, V-pol) + 1550 nm (idler, V-pol), in which the contribution of signal and idler photon pairs generated from clockwise and anti-clockwise directions results in a polarization-entangled state. More details about this source, along with the losses of different fiber optical components, are discussed in our previous work.[28] The signal (shorter-wavelength) and idler (longer-wavelength) photons are separated into the C- (~1520 to 1550 nm) and L- (~1550 to 1580 nm) arms, respectively, of a telecom C–L band splitter. A pair of fiber polarization controllers are used in the C- and L-arms to control the output polarization and to introduce a desired phase in two paths followed by a polarization analyzer setup, which is a combination of a quarter-wave plate (QWP), half-wave plate (HWP), and fiber polarization beam splitter (FPBS). The entangled photon pairs are then combined into a single fiber through another C–L band splitter/combiner. Eventually, we route/demultiplex the entangled photons into various ITU channels using an AWG with a channel separation of 100 GHz. The quantum state fidelity, two-photon interference, and violation of CHSH-Bell's inequality are then characterized in 14 channel pairs using a set of QWP, HWP, and an FPBS placed in the C- and L-arms. The source is designed in such a manner that once we switch it on, it will generate 14 independent polarization-entangled states, and the entanglement in all 14 channel pairs can be analyzed simultaneously in a single measurement.

Here, we characterize the entanglement in all the channel pairs one by one due to the unavailability of 14 detector pairs. We employ a single pair of single-photon avalanche photodetectors (SPADs) (ID Qube NIR), each with a detection efficiency of 20%, a dead time of 5 μs, timing jitter $\lesssim$200 ps, and dark counts <700 cps to perform the entanglement characterization in all channel pairs. Rather than

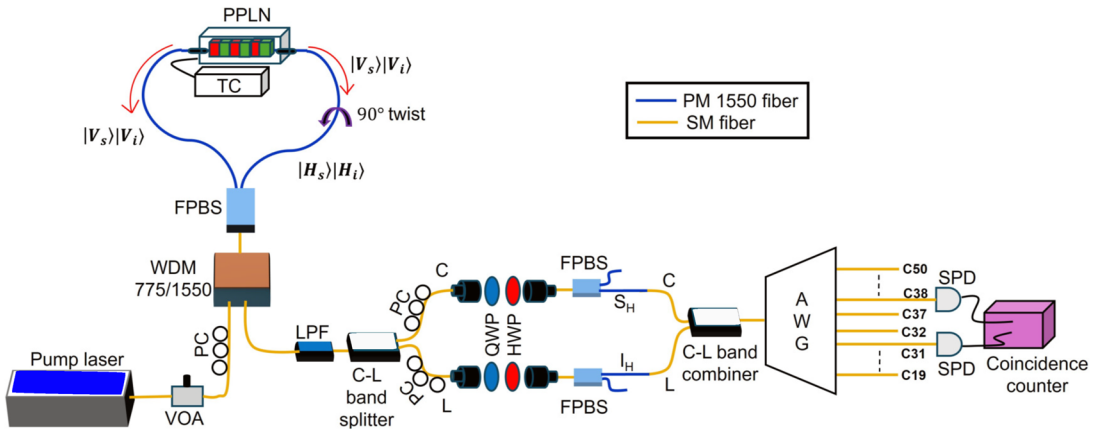

FIG. 1. Experimental setup for polarization-entangled photon pair generation and characterization for multi-user communication at telecom wavelengths. VOA: variable optical attenuator, PC: fiber polarization controller, WDM: wavelength-division-multiplexer, FPBS: fiber polarization beam splitter, TC: temperature controller, LPF: long-pass filter, QWP: quarter wave plate, HWP: half wave plate, SPD: single photon detector, AWG: arrayed waveguide grating, $I_H/|H_i\rangle$: idler with horizontal polarization, $S_H/|H_s\rangle$: signal with horizontal polarization, $|V_i\rangle$: idler with vertical polarization, and $|V_s\rangle$: signal with vertical polarization. The blue and brown lines depict the polarization maintaining and single mode fibers, respectively. C19–C50 are the wavelength channels in the ITU grid (C-band).

optimizing the setup for maximum fidelity in each channel pair, the setup is optimized once, and the measurement is carried out in all channel pairs (sequentially) to see the realistic application of the source. The coincidence events between the two detectors are recorded in a time-tagger unit (PicoQuant, PicoHarp 300) with a time-bin-width of 512 ps.

III. AWG CHARACTERIZATION: CHANNEL PAIR CORRELATION

To implement a source for a multi-user QKD network, the knowledge of channel pair correlation or adjacent channel crosstalk is essential. A high amount of crosstalk deteriorates the entanglement quality of the shared entangled state. This also increases the bit error rate in secret key distribution. Therefore, here we first study the channel pair correlation of the AWG and find the operational parameter of the source at which there is minimum adjacent channel crosstalk. AWG is a single-stage filter that deploys planar waveguide technology, and it consists of two free-propagating regions connected by waveguides. The waveguides have different lengths, leading to constructive or destructive interference of different wavelengths at the output, where each fiber couples out a single wavelength, thus demultiplexing the spectrum.[29] The AWG used in the experiment is a passive optical component with a total of 32 channels from 1537.407 nm (C50) to 1562.23 nm (C19) in the ITU grid. The nominal channel spacing is 100 GHz, and insertion loss in each channel is <3 dB. The actual full width at half-maximum (FWHM) 3-dB bandwidth for each channel pair is slightly non-uniform, i.e., it varies from 26.2 GHz (0.21 nm) to 43.7 GHz (0.35 nm), and polarization-dependent loss is <0.2 dB for each channel pair.

The experimental setup to characterize the channel pair correlations is as follows: A CW pump laser, a VOA, a fiber polarization controller, a type-0 MgO:PPLN waveguide, a WDM at 775/1550 nm, a long-pass filter (LPF), an AWG, an SPAD, and a coincidence counter. We set the pump laser at ~774.8938 nm and operate the waveguide at a phase-matching temperature of 34.33 °C for the single pass downconversion process. The coincidence counts between different wavelength channels of the AWG (i.e., channel pair correlations) are measured in a coincidence counter [see Fig. 2]. It is evident that channel pairs are highly spectrally correlated; e.g., channel number 35 (C35) shows a high coincidence (~666/s) with channel 34 (C34) and a very low coincidence (~18/s) with C33 and ≤2/s with the rest of the channels. Similarly, channel 36 (C36) shows a high coincidence with channel 33 (C33), and so on. We find a very minimum or negligible crosstalk throughout the 16 channel pairs, which indicates that all of them can be used to route the

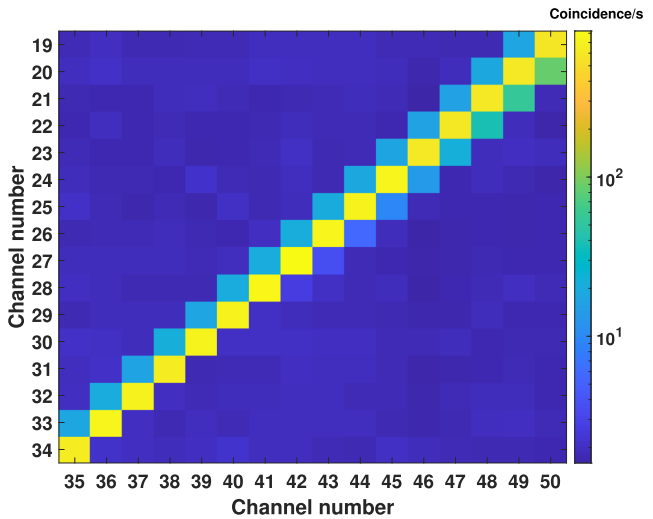

FIG. 2. AWG channel pair correlation at waveguide temperature: 34.33 °C, pump wavelength: 774.8938 nm, and pump power: ~39 μW. The x-axis shows the ITU channels C35 (1549.318 nm) to C50 (1537.407 nm), and the y-axis shows the ITU channels C34 (1550.117 nm) to C19 (1562.23 nm) of AWG. The color bar indicates the coincidence counts/s.

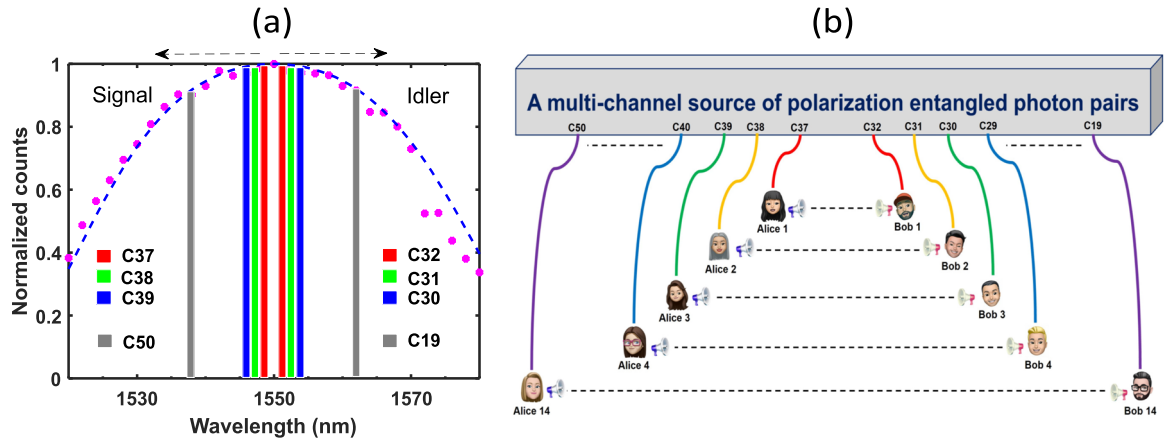

FIG. 3. (a) Photon pair emission spectrum centered around 1550 nm. The pink dots represent the experimental values of photon counts with respect to wavelength, and the dotted blue line is the theoretical sinc^2, Ref. 28. The colored bars show the channels of a 100 GHz channel spacing AWG in the ITU grid. The same color bars around 1550 nm indicate the channel pairs that share an entangled photon pair. (b) Schematic for simultaneous multi-user communication using the source.

entangled photon pairs for multi-user quantum key distribution and communication.

IV. CHANNEL ALLOCATION ON EMISSION SPECTRUM

Figure 3(a) shows the photon pair emission spectrum/bandwidth of the source[28] and the channel pair capacity that can be utilized for quantum communication. The pink dots represent the experimentally measured photon pair emission spectrum, and the dashed blue line is the theoretical sinc^2 distribution. The emission peaks at the degenerate wavelength of ~1550 nm, and the colored bars are the channel wavelengths of AWG. The photon emission spectrum is demultiplexed through the AWG, and the spectrally correlated and polarization-entangled photons enter into these ITU channels. The red, green, and blue bars on the signal side correspond to channels 37 (C37 = 1547.721 nm), 38 (C38 = 1546.921 nm), and 39 (C39 = 1546.125 nm), respectively. The gray color bar shows channel number 50 (C50 = 1537.407 nm). On the idler side, the color bars in the same sequence correspond to channel numbers 32 (C32 = 1551.724 nm), 31 (C31 = 1552.538 nm), 30 (C30 = 1553.322 nm), and 19 (C19 = 1562.23 nm), respectively. The same color bars indicate an entangled photon pair; for example, photons of channel C37 are entangled with the photons of C32, and similarly, photons of channel pair C50 and C19 are entangled. These 14 ITU channel pairs can be provided to 14 different user pairs for simultaneous quantum communication or key distribution [see Fig. 3(b)], and thus, the source acts as a multi-user source. We characterize the entanglement in 14 channel pairs (C37–C32 to C50–C19) of the AWG that are restricted to the highly efficient region of the emission spectrum. Figure 3(a) indicates that more channel pairs can be exploited for quantum communication/key distribution since a large portion of the emission spectrum is still not utilized by our AWG.

V. POLARIZATION ENTANGLEMENT

A. Generation of tunable Bell states

To generate a polarization-entangled Bell state, we pump the waveguide (at T = 34.33 °C) in the Sagnac configuration via an FPBS (see Fig. 1). The probability amplitudes of photon pair generation from the clockwise and anti-clockwise directions add up after the input FPBS in the same mode to generate a symmetric polarization entangled state,

$$|\Phi^+\rangle = \frac{1}{\sqrt{2}}(|H_s\rangle|H_i\rangle + |V_s\rangle|V_i\rangle). \quad (1)$$

The maximally entangled Bell state is accomplished by precisely controlling the input pump polarization and setting an equal path length for the polarization-maintaining fibers on both sides of the waveguide. We first attenuate the waveguide input pump (λ = 774.8938-nm) power to ~50 μW using a VOA and then use an input fiber polarization controller to adjust the pump polarization for the $|\Phi^+\rangle$ Bell-state generation. The photon emission spectrum is split into two halves at about 1550 nm using a commercial C–L band splitter, and a set of manual fiber polarization controllers is used to compensate for the polarization rotation in the two arms (C and L) and to introduce a desired phase difference in the signal and idler photons. We use a set of polarization analyzer tools (QWPs, HWPs, and FPBSs) in the two paths before combining the signal and idler photons via another C–L band splitter/combiner. Finally, the photon pairs are demultiplexed into different ITU channels using a commercially available AWG. This structure allows us to characterize the entanglement in all channel pairs at once without altering the setup. Here, we select only 14 channel pairs (from C37–C32 to C50–C19) for entanglement characterization, leaving out C35–C34 and C36–C33 due to the C–L band splitter's substantial uneven insertion loss at those wavelengths as a result of the device's transmission spectrum.

The experimental setup can also be tuned to generate the $|\Phi^-\rangle$ Bell state,

$$|\Phi^-\rangle = \frac{1}{\sqrt{2}}(|H_s\rangle|H_i\rangle - |V_s\rangle|V_i\rangle). \quad (2)$$

The approach is simply based on the fact that a unitary transformation on one of the qubits of a Bell state can convert it to another Bell state.[30] The $|\Phi^+\rangle$ Bell state can be converted into the $|\Phi^-\rangle$ Bell state if we use a HWP at 0° (i.e., the fast axis of the HWP is aligned

at an angle of 0° with respect to the horizontal axis) in front of either the signal or idler polarization analysis tool. In our case, we achieve this desired phase between the C (signal) and L (idler) arms to convert one state to another with the help of two fiber polarization controllers placed at the end of the first C–L band splitter. Here, we characterize the source for both the entangled states represented by Eqs. (1) and (2).

B. Quantum state characterization

We optimize the source for the maximally entangled two-qubit Bell state generation in channel pair C38–C31 and investigate the entanglement corresponding to both the generated states. Figures 4(a) and 4(b) show the two-photon interference in channel pair C38–C31 for the $|\Phi^-\rangle$ and $|\Phi^+\rangle$ Bell states, respectively. The idler photons traveling in the L-arm are projected into horizontal/vertical (H/V) and diagonal/anti-diagonal (D/A) bases using a HWP and an FPBS; the polarization of signal photons traveling in the C-arm is continuously varied by rotating the corresponding HWP, and a coincidence is recorded between the two photons during this process. We notice that for the $|\Phi^-\rangle$ Bell state, while measuring in the D/A basis, the maximum coincidence occurs when the idler photon is projected into D-polarization and the signal is A-polarized. Whereas for the $|\Phi^+\rangle$ Bell state, the maximum coincidence occurs when the signal is also D-polarized, certifying the generation of two different Bell states. The behavior of interference for the $|\Phi^-\rangle$ and $|\Phi^+\rangle$ Bell states is similar in the H–V basis and is opposite in the D–A basis. In Figs. 4(a) and 4(b), the dots stand for experimental values, and the dashed lines are the sinusoidal fit. The fringe visibilities are 95.98%, 88.23%, 96.91%, and 89.38% for H (0°), D (22.5°), V (45°), and A (67.5°) polarization projections, respectively, for the $|\Phi^-\rangle$ Bell state. For the $|\Phi^+\rangle$ Bell state, the corresponding visibilities are 86.71%, 94.07%, 97.71%, and 90.01%.

Figures 4(c) and 4(d) show the reconstructed density matrices for the $|\Phi^-\rangle$ and $|\Phi^+\rangle$ Bell states, respectively, in channel pair C38–C31. The real and imaginary parts of the density matrices are calculated from the experimental coincidences observed in the quantum state tomography (QST) of the generated Bell state. The raw fidelities for the $|\Phi^-\rangle$ and $|\Phi^+\rangle$ Bell states are ~94% and ~95%, respectively. This shows that the source can generate both the Bell states with high fidelity, and the output state can be easily tuned from $|\Phi^-\rangle$ to $|\Phi^+\rangle$ or vice versa with the help of fiber-based polarization controllers.

C. Entanglement measurement in all channel pairs

For the scaling of a WDM-based quantum communication network, the source must have the capacity to employ a large number of users. This will reduce the total number of sources required to build such a network and also the financial cost of infrastructure.[2]

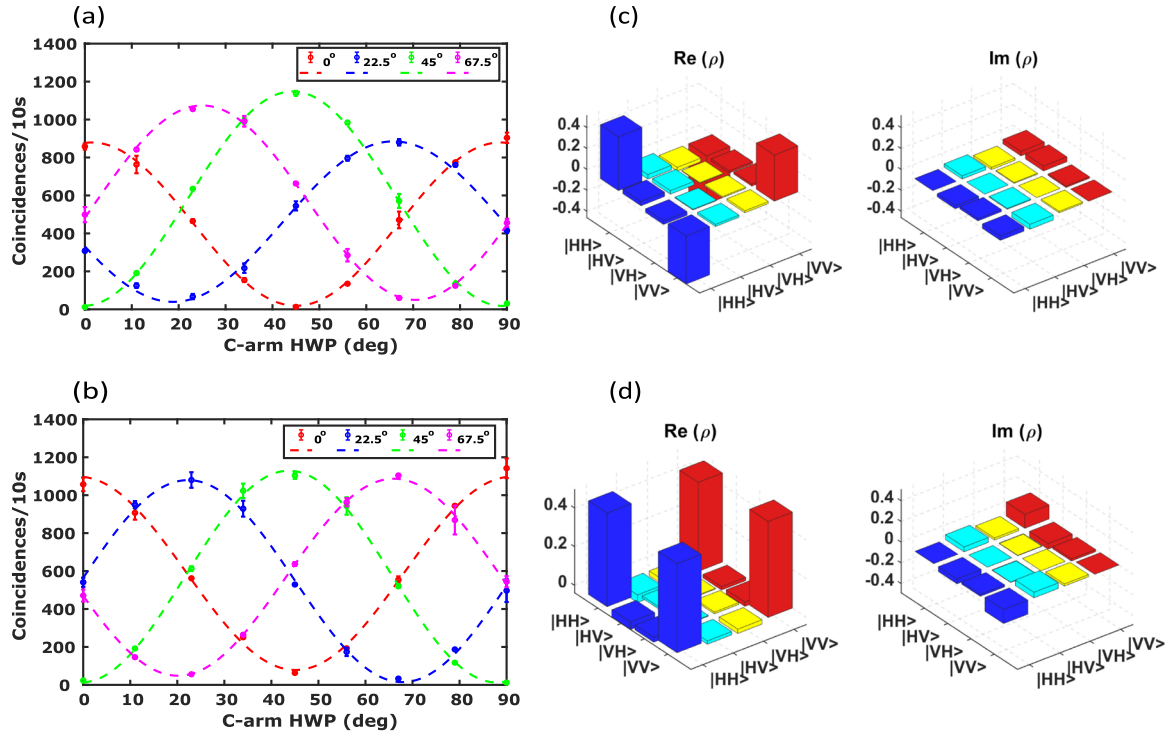

FIG. 4. Two-photon interference for (a) $|\Phi^-\rangle$ Bell state and (b) $|\Phi^+\rangle$ Bell state in the ITU channel pair C38 (1546.921 nm)–C31 (1552.538 nm). The dots and the dashed lines show the experimental data and sinusoidal fit, respectively. Real and imaginary parts of a reconstructed density matrix obtained via quantum state tomography for the (c) $|\Phi^-\rangle$ Bell state, and (d) $|\Phi^+\rangle$ Bell state in the ITU channel pair C38–C31. Raw fidelities for the Bell states $|\Phi^-\rangle$ and $|\Phi^+\rangle$ are ~94% and ~95%, respectively. The density matrix's various colors are intended for the presentation and do not reflect any information.

The hardware needed for simultaneous quantum communication between multi-users can be reduced when a large number of wavelength channels of the source are exploited, enabling all users to be fully connected such that each user shares entanglement with every other user.[1,2] In this regard, we evaluate the capacity of our source and the number of channel pairs that can be used for secure communication, QKD, and entanglement transmission to remote users. Here, we measure the violation of the CHSH inequality, concurrence, and entanglement fidelity by performing QST in 14 channel pairs without altering the experimental setup.

We optimize the source once for channel pair C38–C31 and then use one pair of single-photon detectors (SPADs) to characterize all the entanglement witness parameters in all the channel pairs sequentially. Figures 5(a)–5(c) show the fidelity of the quantum state, concurrence, and S-parameter, respectively, for both $|\Phi^-\rangle$ and $|\Phi^+\rangle$ Bell states in the 14 ITU channel pairs (C37–C32 to C50–C19).

It is evident that the generated state is a high-quality quantum state for all the channel pairs. The raw fidelity is >90% in all channel pairs for the $|\Phi^-\rangle$ Bell state, and the maximum fidelity is ~94% in channel pairs C38–C31 and C39–C30. For the $|\Phi^+\rangle$ Bell state, the raw fidelity is $\gtrsim$89% in all channel pairs, and the maximum fidelity is ~95% in channel pair C38–C31. The raw concurrence is $\gtrsim$0.82 in all channel pairs for the $|\Phi^-\rangle$ Bell state, and the maximum value is ~0.88 in channel pairs C38–C31 and C39–C30. For the $|\Phi^+\rangle$ Bell state, the raw concurrence is $\gtrsim$0.8 in all channel pairs, and the maximum concurrence is ~0.91 in channel pair C38–C31. It is obvious from Fig. 5(c) that each channel pair carries an entangled photon pair substantially violating the CHSH-Bell's inequality (i.e., S > 2) by many standard deviations. The minimum value of the S-parameter is ~2.65 ± 0.03, and the maximum value is ~2.75 ± 0.03 for the $|\Phi^-\rangle$ Bell state; and for the $|\Phi^+\rangle$ state, the minimum value is ~2.56 ± 0.04, and the maximum value is ~2.68 ± 0.03.

These results show that all 14 channel pairs carry an independent bipartite entangled state given by

$$|\Phi_n^{\pm}\rangle = \frac{1}{\sqrt{2}}\left(|H_{\lambda_{n,s}}\rangle|H_{\lambda'_{n,i}}\rangle \pm |V_{\lambda_{n,s}}\rangle|V_{\lambda'_{n,i}}\rangle\right), \tag{3}$$

where $n = 1, 2, 3, \ldots, 14$ and $|H_{\lambda_{n,s}}\rangle$ and $|H_{\lambda'_{n,i}}\rangle$ denote the horizontally polarized signal and idler photons of the nth wavelength channel pair having a wavelength of λ_n and λ'_n, respectively; $|V_{\lambda_{n,s}}\rangle$ and $|V_{\lambda'_{n,i}}\rangle$ denote the vertically polarized signal and idler photons of the nth wavelength channel pair having a wavelength of λ_n and λ'_n, respectively. Each channel pair has unique wavelengths and negligible crosstalk, indicating the parallel generation of 14 independent bipartite entangled states that can be exploited in a WDM-based quantum communication network.

As shown in Fig. 3(b), 14 user pairs can access the source simultaneously for communication/secret key distribution if we deploy a two-user communication scheme. Alice 1 can communicate with Bob 1, Alice 2 can communicate with Bob 2, and so on, since each user pair owns a unique bipartite entangled state independent of the other user pair. Alice 1 cannot communicate with any other user except Bob 1 since they do not share any entangled photons. However, this can be enabled if we use optical switches to route the photons of Bob 1 to any other user with whom Alice 1 wants to communicate,[4] and further, all the channels can be multiplexed to form a complete network where each user shares entanglement with every other user.[1,2] The latter scheme allows any user to communicate with any other user.

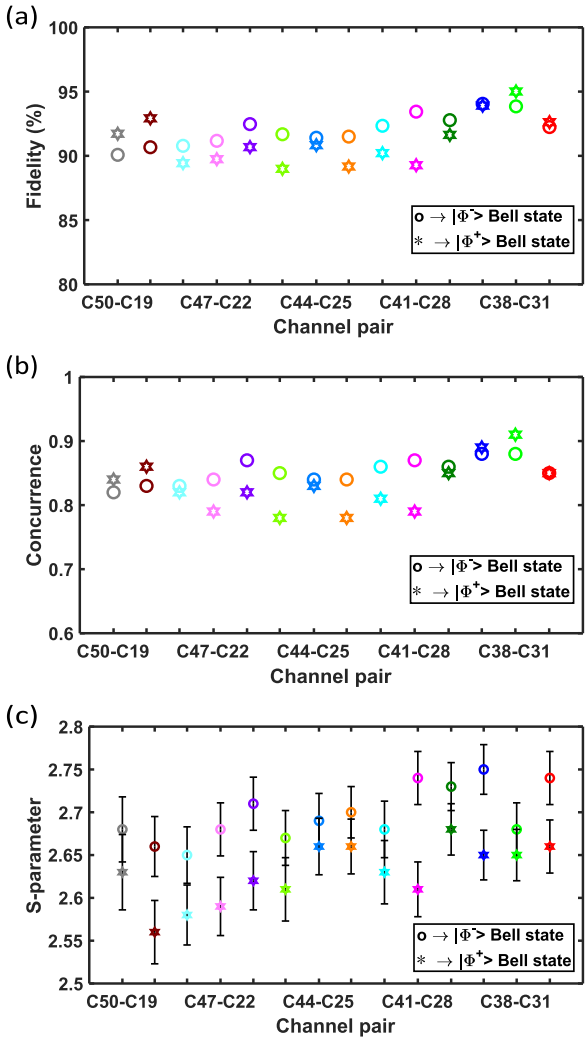

FIG. 5. The raw (a) fidelity, (b) concurrence, and (c) S-parameter for the $|\Phi^-\rangle$ and $|\Phi^+\rangle$ Bell states in 14 different ITU channel pairs. Here, the circles correspond to the $|\Phi^-\rangle$ state, and hexagons (stars) correspond to the $|\Phi^+\rangle$ Bell state. The x-axis shows the ITU channel pairs. All 14 channel pairs indicate the generation of a quantum/entangled state because the fidelity, concurrence, and S-parameter values are more than enough to claim the state as a quantum state.

VI. LONG DISTANCE TRANSMISSION AND QKD

The source needs to be highly efficient to transfer the entangled photons to remote parties for quantum communication[16] and key distribution.[31] In a realistic scenario, the users of a quantum network will typically be located dozens of kilometers apart; therefore, the source must be able to send entangled photons to these far-off users. This requires the multi-user source to have high-fidelity entanglement, high stability, and compactness. We assess our source in this context by observing the fidelity of the transmitted state through

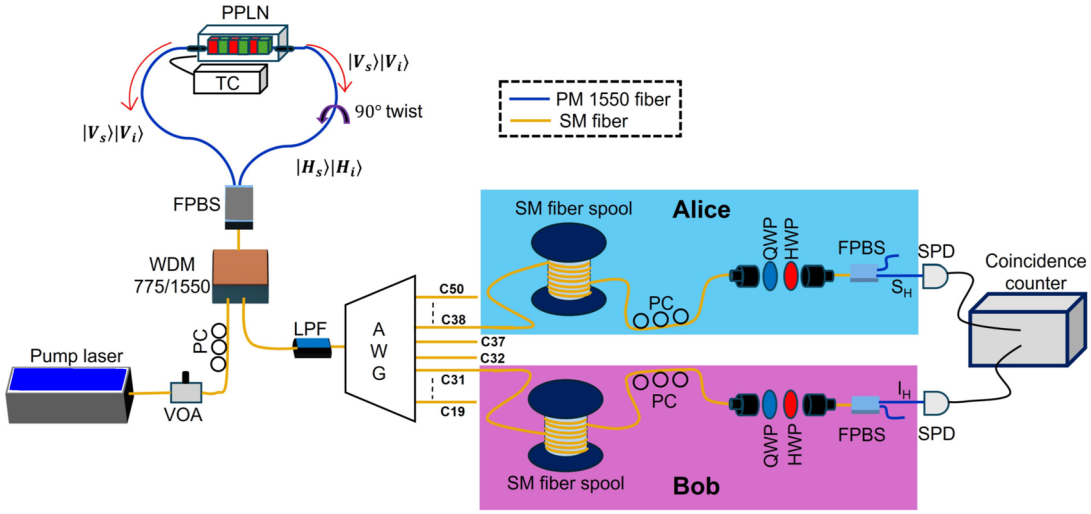

FIG. 6. Experimental setup for long-distance transmission of polarization-entangled photon pairs in a multi-user source for quantum key distribution and communication at telecom wavelength. VOA: variable optical attenuator, PC: fiber polarization controller, WDM: wavelength-division-multiplexer, FPBS: fiber polarization beam splitter, TC: temperature controller, LPF: long-pass filter, AWG: arrayed waveguide grating, SM fiber spool: single mode fiber spool, QWP: quarter wave plate, HWP: half wave plate, SPD: single photon detector, $I_H/|H_i\rangle$: idler with horizontal polarization, $S_H/|H_s\rangle$: signal with horizontal polarization, $|V_i\rangle$: idler with vertical polarization, and $|V_s\rangle$: signal with vertical polarization. The blue and brown lines show the polarization maintaining and single mode fibers, respectively. The coincidences are measured in a Swabian time tagger unit with a 512 ps detection window.

long-distance fiber spools (Sterlite Technologies Ltd.). We observe the impact on coincidence rate, state fidelity, and quantum bit error rate (QBER) when these entangled photon pairs are sent over a long distance.

Since we have already characterized and verified the entanglement in all channel pairs, we now exclude the two C–L band splitters and directly connect the AWG to the LPF, as this will allow us to exploit all the 16-channel pairs of the AWG and would mimic a more realistic scenario where each user pair of the multi-user entangled photon pair source will have their separate polarization analysis module for characterization and key distribution. Figure 6 shows the experimental setup for long-distance transmission of entangled photon pairs. Here, we select the ITU channel pair C38–C31 for one user pair, Alice and Bob, respectively, and connect a fiber spool in one or both channels and characterize the entanglement. We study three different scenarios: (a) when C38 and C31 both have 50 km fiber spools; (b) C31 has a 50 km fiber spool, and C38 does not have any fiber spool; and (c) C31 has a 100 km fiber (serial connection of two 50 km fiber spools), and C38 does not have any fiber spool. In scenario (a), the two spools have a total insertion loss of 13.7 and 13.5 dB, respectively; in scenario (b), the C31 fiber spool has an insertion loss of 13.5 dB; and in scenario (c), these two 50 km fiber spools are connected together to make a distance of 100 km. The above-mentioned losses of the spools contain the propagation loss of the fiber spool and a small (few cm long) FC/APC terminated fiber

TABLE I. Measurement of coincidence rate, fidelity (F), concurrence (C), and quantum bit error rate (QBER) for three combinations of fiber spools in ITU channel pair C38 (Alice)—C31 (Bob) for long-distance transmission of polarization-entanglement. For cases 2 and 3, when no fiber spool is used in channel C38, an equivalent electronic delay is observed in the coincidence peak and accounted for. Alice and Bob's photons are detected using InGaAs APDs (ID Qube NIR), each with a detection efficiency of 20%, a dead time of 5 μs, and dark counts <700 cps, and the coincidence events are counted using the Swabian time tagger X.

S.N.	Case	Coincidence rate	F	C	QBER
1	Alice: 50 km fiber Bob: 50 km fiber	25/s	87.2%	0.82	5%
2	Alice: no fiber Bob: 50 km fiber	120/s	86.8%	0.79	6.4%
3	Alice: no fiber Bob: 100 km fiber	18/s	85.1%	0.71	9%

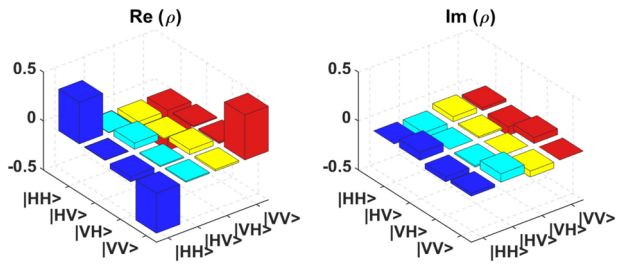

FIG. 7. Real and imaginary part of the density matrix of a $|\Phi^-\rangle$ Bell state after transmitting one photon (i.e., Bob's photon) through a 100 km distance via fiber spool. Here, we use ITU channel pair C38–C31 for long-distance transmission of an entangled photon pair to one user pair. The fidelity and concurrence are ~85.1% and 0.71, respectively.

TABLE II. Comparison of our source with the relevant state-of-the-art multi-user polarization entangled photon-pair sources. NR: not reported, APD: avalanche photodetector, and SNSPD: superconducting nanowire single-photon detector.

Source	Channel pairs for which entanglement demonstrated	Fidelity	Concurrence	S-parameter	Distance up to which entanglement distributed	QBER	Type of detector used
Reference 1	6 (C32–C36, C31–C37, . . ., C27–C41)	>97%[a]	NR	NR	NR	NR	APD
Reference 2	8 (C33–C35, C32–C36, . . ., C26–C42)	NR	NR	NR	~17 km	<6%	SNSPD
Reference 3	6[b]	>90%	NR	NR	NR	NR	NR
Reference 4	4 (C33–C35, C31–C37, . . ., C27–C41)	>92%	NR	NR	NR	<3%	APD
Reference 23	5 (C14–C29, C13–C30, . . ., C10–C33)	>85%	NR	2.72 ± 0.02[c]	NR	NR	APD
References 24,25	15 (C33–C35, C32–C36, . . ., C19–C49)	NR	NR	NR	5.6 km	<1%	SNSPD/APD
This work	14 (C32–C37, C31–C38, . . ., C19–C50)	>90%[d] (max ~ 94%)	>0.8[d] (max ~ 0.88)	>2.65 ± 0.03[d] (max 2.75 ± 0.03)	50 km 100 km	<5% <9%	APD

[a]Setup was optimized for each channel pair to achieve maximum fidelity.
[b]Six channel pairs were selected between Ch1 (signal = 1525 nm, idler = 1580 nm) and Ch44 (signal = 1545.3 nm, idler = 1558.8 nm).
[c]Max value.
[d]For $|\Phi^-\rangle$ Bell state.

patch cord that is fiber spliced to the spool on both ends. The entanglement measurement results are listed in Table I. In all the cases, the fidelity is >85%, and QBER is <9% (below the generally accepted 11% threshold for error-correction[32,33]), which shows that the high-quality entangled photon pairs can be transmitted to remote users for communication and key distribution. The reconstructed density matrix for the case when Bob's photon is transmitted 100 km and Alice's photon is detected just after the AWG channel C38 is shown in Fig. 7. The above results highlight the quality of our source for long-distance multi-user quantum communication. A comparison of our source with the relevant state-of-the-art multi-user sources is shown in Table II. All the results described in this paper are measured with conventional APDs, and these are the best reported with these detectors for such a large number of channel pairs. The performance of our source would be much better if it were measured using state-of-the-art SNSPDs.

VII. EFFECT OF POLARIZATION MODE DISPERSION

Polarization mode dispersion (PMD) can cause entanglement degradation in optical fiber-based quantum communication.[34] PMD is caused by the birefringence in the optical medium, where two orthogonal polarizations travel at different speeds, resulting in differential delay/walk-off. PMD is a concern in optical fiber-based quantum networks for entanglement distribution among distant users due to the introduction of distinguishability between the two polarization components in each photon, leading to degradation in entanglement.[34–36] Single-mode fibers in the submarine cable environment or aerial exposure experience stress, sudden change in temperature, or change in ambient condition, which induces birefringence, hence PMD, resulting in the deterioration of the quality of the entangled state.[37] Thus, it is necessary to understand the effect of PMD on polarization entanglement for effective quantum communication among distant users. Here, we measure the change in the concurrence (C) parameter of the entangled state if we use different-length single-mode fibers for the two channels/users using a setup similar to Fig. 6. The fibers have a PMD value of 0.1 ps/$\sqrt{\text{km}}$ and chromatic dispersion of ≤17.5 ps/nm km according to the specification sheet. It is observed that the concurrence does not change much even if we keep a fiber length difference of 100 km between the two remote users [see Fig. 8(a)], which is also suggested by the theory in the absence of any external environmental introduced stresses.[36] The dots represent the experimentally measured values, and the blue lines show the theoretical results. The solid blue line corresponds to the case when we consider a PMD value of 0.1 ps/$\sqrt{\text{km}}$ in single-mode fiber, and the dotted blue line corresponds to the case when we consider a PMD value of 0.35 ps/$\sqrt{\text{km}}$. Our experimental result agrees well with the theory, which is modeled from Ref. 36 for a CW pump scenario. The theoretical concurrence is calculated using

$$C(\tau_a, \tau_b) = \exp\left(-\frac{1}{2}\frac{(\tau_a - \tau_b)^2 B_a^2 B_b^2}{B_a^2 + B_b^2}\right), \tag{4}$$

where $\tau_{a,b}$ is the differential group delay (DGD) and $B_{a,b}$ is the filter bandwidth of Alice and Bob's path, respectively. Our experimental result slightly deviates from the solid blue line and matches more with the dotted blue line (high PMD value[38]). We note that the drop in concurrence with fiber length could also have contributions from polarization-dependent loss (PDL), chromatic dispersion, and wavelength-dependent loss (although expected to be small), and this probably requires a more detailed study on its own. Nonetheless, this suggests that stable single-mode fibers, such as the submarine fibers, will not degrade the entanglement significantly and will require very slow live adjustment. Meanwhile, aerial fibers will require faster

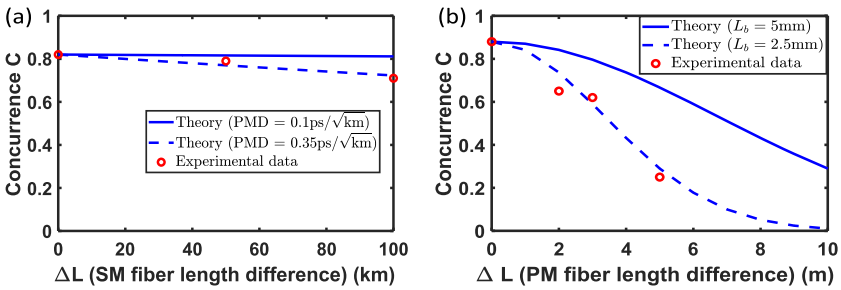

FIG. 8. (a) Variation of concurrence with single-mode (SM) fiber length difference (PMD) in two channels (C38, C31). (b) Variation of concurrence with polarization-maintaining (PM) fiber length difference (PMD) in two channels (C38, C31). The solid and dotted blue lines are the theoretical estimates, and the red dots are the experimental values. L_b is the beat length of PM 1550 fiber.

compensation systems for stability.[16] In order to see the effect of high PMD on concurrence, we put polarization-maintaining fiber patch cords of different lengths in channels C38 and C31 instead of single-mode fiber spools. It is observed that the concurrence drops significantly even with a very small fiber length difference in the two channels [see Fig. 8(b)]. The red dots in Fig. 8(b) correspond to the experimental data, and the blue lines are the theoretical results. The solid blue line pertains to the case when we consider a beat length (L_b) of 5 mm for PMD in these polarization-maintaining fibers, which is also claimed by the manufacturer, and the dotted blue line pertains to the case when we take a beat length of 2.5 mm. Our experimental values slightly deviate from the theoretical curve (solid blue line) and agree well with the dotted blue line. This study suggests that an increase in PMD deteriorates the entanglement quality rapidly, and the single-mode fibers encased in stable cables are an excellent medium to safely transfer the polarization entanglement to remote users for communication or key distribution in a quantum network.

VIII. CONCLUSION

We have characterized a fully fiber-integrated multi-user source of polarization-entangled photon pairs in the telecom C-band. The source is based on a fiber-pigtailed type-0 SPDC in a Zn-indiffused MgO:PPLN ridge waveguide placed in Sagnac configuration, and it can be easily tuned with the help of a fiber-polarization controller to generate either $|\Phi^+\rangle$ or $|\Phi^-\rangle$ Bell state. We generate 14 independent bipartite entangled states simultaneously through the demultiplexing of the emission spectrum using a telecom DWDM AWG, which can be used by 14 different user pairs for quantum communication or secure key distribution. The entanglement is analyzed in all 14 ITU channel pairs (C37–C32 to C50–C19) for both $|\Phi^+\rangle$ and $|\Phi^-\rangle$ Bell states. The interference fringe visibilities corresponding to the $|\Phi^-\rangle$ Bell state in the ITU channel pair C38–C31 are >95% and >88% in the H–V and D–A basis, respectively, whereas for the $|\Phi^+\rangle$ Bell state the corresponding visibilities are >86% and >90%. In all channel pairs, the raw fidelity is >90% for the $|\Phi^-\rangle$ Bell state, and the maximum fidelity is ~94% corresponding to the channel pairs C38–C31 and C39–C30. For the $|\Phi^+\rangle$ Bell state, the raw fidelities are $\gtrsim$89% for all the channel pairs, and the maximum fidelity is ~95% corresponding to the channel pair C38–C31. The raw concurrence for both the Bell states ($|\Phi^-\rangle$ and $|\Phi^+\rangle$) is $\gtrsim$0.8 (in all channel pairs), and the maximum values are ~0.88 and ~0.91, pertaining to channel pair C38–C31. The observed S-parameter is >2.56 ± 0.04 in all the channel pairs for both the Bell states, which highlights that all 14 ITU-channel pairs violate the CHSH-Bell's inequality and contain high-fidelity entangled states. Our source's architecture allows us to characterize the entanglement in all channel pairs at once without disturbing the setup, which is requisite for a realistic quantum communication network where the service provider has to switch on the source once for high-fidelity multi-user communication. Our source is highly robust and can be employed in a WDM quantum communication network.

We further demonstrate entanglement distribution up to 100 km using single-mode fiber spools (having a total fiber loss of 27.2 dB) in channel pair C38–C31. The high fidelity (>85%) and low QBER (<9%) value suggest that the source can potentially be used for long-distance multi-user communication and secure key distribution, owing to the low transmission loss of fibers around 1550-nm. We also study the effect of PMD in long-distance entanglement transmission using single-mode as well as polarization-maintaining fibers. The latter is found to degrade the entanglement much quicker than the former. In the case of single-mode fibers, even a very large difference in fiber length between the two remote users can be tolerated as the concurrence does not change significantly in the absence of large environmental stresses. This indicates that single-mode fibers in the shielded cables are the best optical media for entanglement distribution among distant users in a fiber-based quantum communication network. Here, we have shown only 14 independent channel pairs of entangled photons, but more channels (up to ~40 channel pairs with 100-GHz spacing) can be exploited since a large part of the photon emission spectrum is still left unused. These independent channel pairs can be multiplexed to form a complete network where each user shares entanglement with the rest,[1,2] allowing communication between any two parties as desired. We have demonstrated a fully fiber-integrated source with full characterization of 14 independent but simultaneous bipartite polarization-entangled states for long-distance multi-user communication/key distribution using standard room temperature APDs, and this proposed source can be a potential candidate for long-distance transmission of entangled photons, multi-user communication, and secure key distribution over a metro-area WDM quantum network. The source can potentially have more applications in quantum communication and networking where entangled and/or correlated photons are required, such as information processing, entanglement swapping, and quantum teleportation.

ACKNOWLEDGMENTS

We thank Sterlite Technologies Ltd. and Professor Amol Choudhary, Department of Electrical Engineering, Indian Institute

of Technology Delhi, New Delhi, India, for providing the single-mode fiber spools for long-distance entanglement transmission measurement. The authors acknowledge the Department of Science and Technology, India, for the project grant (No. DST/ICPS/QuST/Theme-1/2019/Q-62) and the Council of Scientific and Industrial Research, India, for the senior research fellowship [No. 09/086(1351)/2018-EMR-I] of V.K.Y.

AUTHOR DECLARATIONS

Conflict of Interest

The authors have no conflicts to disclose.

Author Contributions

Vikash Kumar Yadav: Conceptualization (equal); Data curation (lead); Formal analysis (lead); Investigation (equal); Methodology (equal); Visualization (lead); Writing – original draft (lead); Writing – review & editing (equal). **Vivek Venkataraman**: Conceptualization (equal); Investigation (equal); Methodology (equal); Supervision (lead); Validation (equal); Visualization (equal); Writing – review & editing (equal). **Joyee Ghosh**: Conceptualization (equal); Funding acquisition (lead); Investigation (equal); Methodology (equal); Project administration (lead); Resources (lead); Supervision (lead); Validation (equal); Visualization (equal); Writing – review & editing (equal).

V.K.Y. built the experimental setup and performed the experiment. V.K.Y. also analyzed the data and wrote the original manuscript. V.V. and J.G. reviewed the manuscript and supervised the project. All authors discussed the results and commented on the manuscript.

DATA AVAILABILITY

The data that support the findings of this study are available from the corresponding author upon reasonable request.

REFERENCES

[1]S. Wengerowsky, S. K. Joshi, F. Steinlechner, H. Hübel, and R. Ursin, "An entanglement-based wavelength-multiplexed quantum communication network," Nature **564**, 225–228 (2018).
[2]S. K. Joshi, D. Aktas, S. Wengerowsky, M. Lončarić, S. P. Neumann, B. Liu, T. Scheidl, G. C. Lorenzo, Ž. Samec, L. Kling *et al.*, "A trusted node–free eight-user metropolitan quantum communication network," Sci. Adv. **6**, eaba0959 (2020).
[3]H. C. Lim, A. Yoshizawa, H. Tsuchida, and K. Kikuchi, "Broadband source of telecom-band polarization-entangled photon-pairs for wavelength-multiplexed entanglement distribution," Opt. Express **16**, 16052–16057 (2008).
[4]I. Herbauts, B. Blauensteiner, A. Poppe, T. Jennewein, and H. Hübel, "Demonstration of active routing of entanglement in a multi-user network," Opt. Express **21**, 29013–29024 (2013).
[5]R. Ursin, F. Tiefenbacher, T. Schmitt-Manderbach, H. Weier, T. Scheidl, M. Lindenthal, B. Blauensteiner, T. Jennewein, J. Perdigues, P. Trojek *et al.*, "Entanglement-based quantum communication over 144 km," Nat. Phys. **3**, 481–486 (2007).
[6]V. Scarani, H. Bechmann-Pasquinucci, N. J. Cerf, M. Dušek, N. Lütkenhaus, and M. Peev, "The security of practical quantum key distribution," Rev. Mod. Phys. **81**, 1301 (2009).
[7]X. Ma, C.-H. F. Fung, and H.-K. Lo, "Quantum key distribution with entangled photon sources," Phys. Rev. A **76**, 012307 (2007).
[8]A. K. Ekert, "Quantum cryptography based on Bell's theorem," Phys. Rev. Lett. **67**, 661 (1991).
[9]C. H. Bennett, G. Brassard, and N. D. Mermin, Phys. Rev. Lett. **68**, 557 (1992).
[10]D. Bouwmeester, J.-W. Pan, K. Mattle, M. Eibl, H. Weinfurter, and A. Zeilinger, "Experimental quantum teleportation," Nature **390**, 575–579 (1997).
[11]Y. Li, Y. Huang, T. Xiang, Y. Nie, M. Sang, L. Yuan, and X. Chen, "Multiuser time-energy entanglement swapping based on dense wavelength division multiplexed and sum-frequency generation," Phys. Rev. Lett. **123**, 250505 (2019).
[12]V. Giovannetti, S. Lloyd, and L. Maccone, "Advances in quantum metrology," Nat. Photonics **5**, 222–229 (2011).
[13]S. Pirandola, B. R. Bardhan, T. Gehring, C. Weedbrook, and S. Lloyd, "Advances in photonic quantum sensing," Nat. Photonics **12**, 724–733 (2018).
[14]Z. Zhang, S. Mouradian, F. N. Wong, and J. H. Shapiro, "Entanglement-enhanced sensing in a lossy and noisy environment," Phys. Rev. Lett. **114**, 110506 (2015).
[15]S. Wengerowsky, S. K. Joshi, F. Steinlechner, J. R. Zichi, S. M. Dobrovolskiy, R. Van der Molen, J. W. Los, V. Zwiller, M. A. Versteegh, A. Mura *et al.*, "Entanglement distribution over a 96-km-long submarine optical fiber," Proc. Natl. Acad. Sci. U. S. A. **116**, 6684–6688 (2019).
[16]S. Wengerowsky, S. K. Joshi, F. Steinlechner, J. R. Zichi, B. Liu, T. Scheidl, S. M. Dobrovolskiy, R. v. d. Molen, J. W. Los, V. Zwiller *et al.*, "Passively stable distribution of polarisation entanglement over 192 km of deployed optical fibre," Npj Quantum Inf. **6**, 5 (2020).
[17]T. Scheidl, R. Ursin, A. Fedrizzi, S. Ramelow, X.-S. Ma, T. Herbst, R. Prevedel, L. Ratschbacher, J. Kofler, T. Jennewein, and A. Zeilinger, "Feasibility of 300 km quantum key distribution with entangled states," New J. Phys. **11**, 085002 (2009).
[18]T.-G. Noh, H. Kim, T. Zyung, and J. Kim, "Efficient source of high purity polarization-entangled photon pairs in the 1550nm telecommunication band," Appl. Phys. Lett. **90**, 011116 (2007).
[19]S. Arahira, N. Namekata, T. Kishimoto, H. Yaegashi, and S. Inoue, "Generation of polarization entangled photon pairs at telecommunication wavelength using cascaded $\chi^{(2)}$ processes in a periodically poled $LiNbO_3$ ridge waveguide," Opt. Express **19**, 16032–16043 (2011).
[20]P. Vergyris, F. Kaiser, E. Gouzien, G. Sauder, T. Lunghi, and S. Tanzilli, "Fully guided-wave photon pair source for quantum applications," Quantum Sci. Technol. **2**, 024007 (2017).
[21]N. Matsuda, H. Le Jeannic, H. Fukuda, T. Tsuchizawa, W. J. Munro, K. Shimizu, K. Yamada, Y. Tokura, and H. Takesue, "A monolithically integrated polarization entangled photon pair source on a silicon chip," Sci. Rep. **2**, 817 (2012).
[22]X. Li, P. L. Voss, J. E. Sharping, and P. Kumar, "Optical-fiber source of polarization-entangled photons in the 1550 nm telecom band," Phys. Rev. Lett. **94**, 053601 (2005).
[23]P. Vergyris, F. Mazeas, E. Gouzien, L. Labonté, O. Alibart, S. Tanzilli, and F. Kaiser, "Fibre based hyperentanglement generation for dense wavelength division multiplexing," Quantum Sci. Technol. **4**, 045007 (2019).
[24]R. Wang, O. Alia, M. J. Clark, S. Bahrani, S. K. Joshi, D. Aktas, G. T. Kanellos, M. Peranić, M. Lončarić, M. Stipčević *et al.*, "A dynamic multi-protocol entanglement distribution quantum network," in *2022 Optical Fiber Communications Conference and Exhibition (OFC)* (IEEE, 2022), pp. 1–3.
[25]M. J. Clark, O. Alia, R. Wang, S. Bahrani, M. Peranić, D. Aktas, G. T. Kanellos, M. Loncaric, Ž. Samec, A. Radman *et al.*, "Entanglement distribution quantum networking within deployed telecommunications fibre-optic infrastructure," Proc. SPIE **12335**, 96–103 (2023).
[26]M. J. Clark, "Quantum networking through polarisation entanglement distribution," Ph.D. thesis (University of Bristol, 2024).
[27]V. Kumar Yadav, V. Venkataraman, and J. Ghosh, "Broadband telecom photon pairs from a fiber-integrated PPLN ridge waveguide," Opt. Lett. **47**, 5132–5135 (2022).
[28]V. K. Yadav, V. Venkataraman, and J. Ghosh, "High-brightness fiber-coupled source of polarization-entangled photon pairs spanning the telecom C- and L-bands," Opt Laser. Technol. **175**, 110774 (2024).
[29]H. Takahashi, Y. Hibino, and I. Nishi, "Polarization-insensitive arrayed-waveguide grating wavelength multiplexer on silicon," Opt. Lett. **17**, 499–501 (1992).

[30]N. Kiesel, "Experiments on multiphoton entanglement," Ph.D. thesis (LMU, 2007).
[31]T. Honjo, S. W. Nam, H. Takesue, Q. Zhang, H. Kamada, Y. Nishida, O. Tadanaga, M. Asobe, B. Baek, R. Hadfield *et al.*, "Long-distance entanglement-based quantum key distribution over optical fiber," Opt. Express **16**, 19118–19126 (2008).
[32]A. Acín, N. Brunner, N. Gisin, S. Massar, S. Pironio, and V. Scarani, "Device-independent security of quantum cryptography against collective attacks," Phys. Rev. Lett. **98**, 230501 (2007).
[33]S. Pirandola, U. L. Andersen, L. Banchi, M. Berta, D. Bunandar, R. Colbeck, D. Englund, T. Gehring, C. Lupo, C. Ottaviani *et al.*, "Advances in quantum cryptography," Adv. Opt. Photonics **12**, 1012–1236 (2020).
[34]H.-T. Lim, K.-H. Hong, and Y.-H. Kim, "Effects of polarization mode dispersion on polarization-entangled photons generated via broadband pumped spontaneous parametric down-conversion," Sci. Rep. **6**, 25846 (2016).
[35]M. Brodsky, E. C. George, C. Antonelli, and M. Shtaif, "Loss of polarization entanglement in a fiber-optic system with polarization mode dispersion in one optical path," Opt. Lett. **36**, 43–45 (2011).
[36]M. Shtaif, C. Antonelli, and M. Brodsky, "Nonlocal compensation of polarization mode dispersion in the transmission of polarization entangled photons," Opt. Express **19**, 1728–1733 (2011).
[37]B. Hakki, "Polarization mode dispersion in a single mode fiber," J. Lightwave Technol. **14**, 2202–2208 (1996).
[38]G. P. Agrawal, *Nonlinear Fiber Optics*, 3rd ed. (Academic Press, 2001).